Journal of Coordination Chemistry

ISSN: 0095-8972 (Print) 1029-0389 (Online) Journal homepage: http://www.tandfonline.com/loi/gcoo20

Kinetic and mechanistic studies of the reactivity of iron(IV) TAMLs toward organic sulfides in water: resolving a fast catalysis versus slower single-turnover reactivity dilemma

Deboshri Banerjee, Alexander D. Ryabov & Terrence J. Collins

To cite this article: Deboshri Banerjee, Alexander D. Ryabov & Terrence J. Collins (2015) Kinetic and mechanistic studies of the reactivity of iron(IV) TAMLs toward organic sulfides in water: resolving a fast catalysis versus slower single-turnover reactivity dilemma, Journal of Coordination Chemistry, 68:17-18, 3032-3045, DOI: 10.1080/00958972.2015.1065974

To link to this article: http://dx.doi.org/10.1080/00958972.2015.1065974

Accepted author version posted online: 29 Jun 2015.
Published online: 27 Jul 2015.

Journal of Coordination Chemistry, 2015
Vol. 68, Nos. 17–18, 3032–3045, http://dx.doi.org/10.1080/00958972.2015.1065974

Kinetic and mechanistic studies of the reactivity of iron(IV) TAMLs toward organic sulfides in water: resolving a fast catalysis *versus* slower single-turnover reactivity dilemma

DEBOSHRI BANERJEE, ALEXANDER D. RYABOV* and TERRENCE J. COLLINS*

Department of Chemistry, Carnegie Mellon University, Pittsburgh, PA, USA

(*Received 4 March 2015; accepted 8 June 2015*)

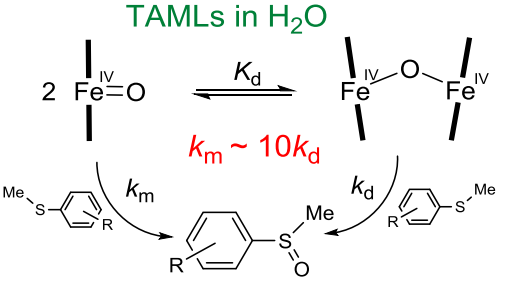

TAML complex $[Fe^{III}\{C_6H_4\text{-}1,2\text{-}(NCOCMe_2NCO)_2CMe_2\}OH_2]^-$ (**1**) is oxidized by H_2O_2 or ^{t}BuOOH in water at pH < 10 into the corresponding iron(IV) μ-oxo-bridged dimer **2**, which oxidizes readily ring-substituted thioanisoles *p*-XC_6H_4SMe (X=H, MeO, Me, Cl, CN) into the corresponding sulfoxides with regeneration of **1**. The oxidation studied under pseudo-first-order conditions using the stopped-flow technique by monitoring the fading of the 420-nm band of **2** follows hyperbolic kinetics according to the rate law $k_{obs} = ab[p\text{-}XC_6H_4SMe]/(1 + b[p\text{-}XC_6H_4SMe])$ at pH 8 and 25 °C. Parameters *a*, *b*, and *ab* all decrease for electron-poorer thioanisoles and the Hammett value $\rho \sim 1$ has been found for *ab*, which can be associated with the second-order rate constants for oxidation of thioanisoles by **2**. The kinetics of oxidation of *p*-$NO_2C_6H_4SMe$ by H_2O_2 catalyzed by **1** has been studied under steady-state conditions. Covering the concentration of **1** in a 100-fold range has revealed that though first-order kinetics in **1** is observed at low catalyst concentrations (below 10^{-6} M), there is a significant negative deviation from linearity at $[\mathbf{1}] > 10^{-6}$ M. The latter was rationalized by the equilibrium between the monomeric and dimeric Fe^{IV} species 2 M ⇌ M–M (K_d), both being able to oxidize *p*-$NO_2C_6H_4SMe$ with rate constants k_m and k_d which were found to be $(13 \pm 1) \times 10^4$ and $(0.32 \pm 0.01) \times 10^4$ M^{-1} s^{-1}, respectively. The difference in the rate constants is the key for resolving the dilemma of faster catalysis *versus* slower single-turnover reactivity of TAML activators in water.

Keywords: Iron complex; TAML; Kinetics; Mechanism; Thioanisoles; Stopped-flow

*Corresponding authors. Email: ryabov@andrew.cmu.edu (A.D. Ryabov); tc1u@andrew.cmu.edu (T.J. Collins)
Dedicated to Prof. Rudi van Eldik on the occasion of his 70th birthday.

1. Introduction

Iron complexes in higher oxidation states have attracted much attention from academic and industrial researchers due to their enormous oxidizing potential in numerous instances [1–7]. Our interests focus on the iron TAML activators of peroxides (TAML = tetraamido macrocyclic ligand or their iron complexes) [8, 9] which have a broad spectrum of environmentally oriented applications [10] and bio-inspired and -competitive mechanistic chemistry [5, 11]. In 2008, we reported that TAML complex **1** (chart 1) is transformed by ^{t}BuOOH in water into iron(IV) derivatives **2** and/or **3** depending on reaction conditions[12, 13]. Later, the kinetics and mechanism of this transformation were explored in detail in collaboration with Professor Rudi van Eldik, to whom this issue is devoted [14]. Our investigations of the reactivity of Fe^{V} and Fe^{IV} complexes derived from TAMLs, which were performed at −40 °C in MeCN, revealed that both forms oxidize thioanisoles, though Fe^{V} is by several orders of magnitude more reactive than Fe^{IV} [15]. More recently, we explored the reactivity of iron(IV) species in aqueous solution toward hexacyanoferrate(II) as an electron donor [16]. Here, we report the results of kinetic and mechanistic studies of the oxidation of ring-substituted thioanisoles into the corresponding sulfoxides under catalytic and single-turnover conditions using conventional and stopped-flow spectroscopy, respectively. The data revealed that Fe^{IV} TAML species behave as electrophiles toward *p*-XC_6H_4SMe and allowed us to rationalize a pseudo-controversial discrepancy in reactivity measured under the catalytic conditions (below micromolar concentrations) and the single-turnover conditions, which require significantly higher concentrations of TAML activators. This effect is ascribed to the reversible formation of less reactive dimeric iron(IV) species, which start to play a noticeable role at TAML concentrations above 10^{-6} M.

2. Experimental

2.1. *Materials and methods*

Thioanisole and *p*-substituted thioanisoles purchased from Sigma and Aldrich were used as received. Orange II (Aldrich) was purified by passing through a column filled with SMT Bulk-C18 (Separation Methods Technologies Inc., Newark) with water–methanol mixture (9 : 1) as an eluent. H_2O_2 (30% w/w) and ^{t}BuOOH (70% w/w in water) were purchased

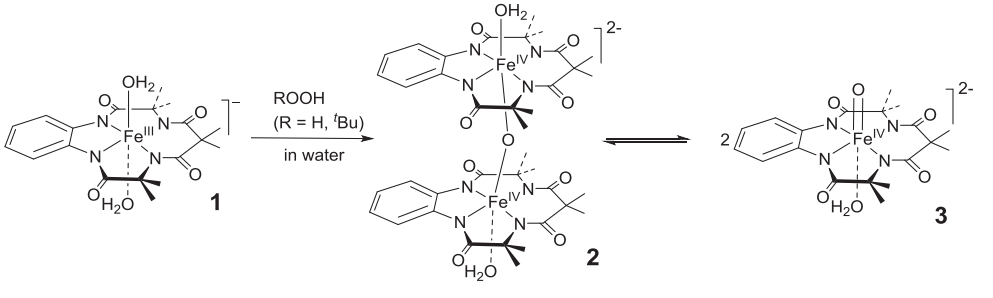

Chart 1. TAML activators used in this study.

from Fluka. Other reagents, components of buffer solutions, and solvents (at least ACS reagent grade) were obtained from Aldrich, Fisher, or Acros and used as received or purified in an appropriate manner [17]. TAML **1** was synthesized as described elsewhere [18]. UV–vis spectrophotometric measurements were performed using a Hewlett Packard diode array spectrophotometer (model 8453) equipped with a thermostated cell holder and an automatic eight-cell positioner. Temperature was controlled by Thermo digital temperature controller RTE17 with an accuracy of ±1 °C. Both quartz and appropriate plastic 1.0-cm cuvettes were used. Stopped-flow kinetic measurements were carried out using a two-syringe BioKine32 SFM-20 model (BioLogic Science Instruments) at 25 °C. Technical details are summarized elsewhere [14]. Products of the oxidation of thioanisoles were analyzed by high-performance liquid chromatography (HPLC) using a Varian C18 Omnispher column with acetonitrile and water as eluting solvents, as well as by gas chromatography–mass spectrometer (GC–MS) using a ThermoDSQ instrument. Kinetic measurements were performed at pH 8 in 0.01-M phosphate buffer prepared using HPLC grade water. Stock solutions of thioanisoles and other substrates used in this study were prepared in acetonitrile (HPLC grade) or buffer/acetonitrile mixture. Stock solution of Orange II was prepared in water (HPLC grade). Stock solutions of H_2O_2 were prepared from 30% H_2O_2 and standardized by measuring the absorbance at 230 nm ($\varepsilon = 72.8\ M^{-1}\ cm^{-1}$) [19]. Fresh stock solutions of ^{t}BuOOH were prepared from 70% ^{t}BuOOH in water (ca. 7.2 M) without calibration. Stock solutions of all TAML catalysts used in this study were made in water (HPLC grade) or acetonitrile (HPLC grade).

2.2. *Reactions of 2*

Solutions of **2** were prepared at 25 °C by adding 0.5 equivalents of H_2O_2 or ^{t}BuOOH to solutions of **1** in 0.01-M phosphate buffer at pH 8.0. Reactions with thioanisoles were followed by monitoring UV–vis spectra of **2** at 420 and 780 nm after addition of variable concentrations of the substrates. Products of the reaction between **2** and thioanisole were analyzed by HPLC and identified by comparing retention times to that of the authentic compound.

2.3. *Kinetic studies*

The kinetics of oxidation of 4-nitrothioanisole was monitored by following its absorbance decrease at 350 nm, while that for Orange II was monitored at 485 nm (pH 8). The temperature was always maintained at 25 °C. A typical kinetic run was performed as follows. The phosphate buffer (2 mL) was first added to a thermostated cuvette to which appropriate amounts of the stock solutions of a substrate and **1** were added. The reaction was initiated by the addition of an aliquot of the stock solution of ^{t}BuOOH or H_2O_2. The rates were calculated from the measured changes in absorbance with time using the estimated extinction coefficients for the substrates.

3. Results and discussion

3.1. *Introductory remarks*

In the solid state, iron(III) TAML compounds are five-coordinate square pyramidal species with an axial aqua, methanolic or acido ligand [5, 11]. In water, they are six-coordinate

diaqua species **1** with axial water ligands as shown in chart 1. A first aqua ligand of **1** deprotonates with pK_a of 10.1 [20]. A half equivalent of H_2O_2 (faster) [14] or ^{t}BuOOH (slower) [12] converts millimolar solutions of **1** in water into an iron(IV) TAML species, which is either the μ-oxo dimer **2** or oxoiron monomer **3** as confirmed by the results of Mössbauer spectroscopy [12]. Species **2**, which is structurally similar to the complex generated from **1** by dioxygen in organic solvents [21], dominates at pH below 10, while species **3** dominates at pH above 12. Variation of pH converts reversibly **2** into **3** and vice versa suggesting the following equilibrium [12]:

$$[\mathrm{LFe{-}O{-}FeL}]^{2-}(\mathbf{2}) + 2\mathrm{OH}^- \leftrightharpoons 2[\mathrm{LFe^{IV}{=}O}]^{2-}(\mathbf{3}) + \mathrm{H_2O} \quad (1)$$

Major spectral differences between **2** and **3** manifest in the visible region at wavelengths above 700 nm where **3** does not absorb light. In contrast, **2** has two broad metal-to-ligand charge transfer bands around 800 and 1100 nm [figure 1(a)]. Equilibrium 1 controlled by hydroxide ions suggests that a similar process as shown by equation (2) may occur at lower pH in *dilute* solutions of **2**.

$$[\mathrm{LFe{-}O{-}FeL}]^{2-}(\mathbf{2}) + \mathrm{H_2O} \leftrightharpoons 2[\mathrm{LFe^{IV}{-}OH}]^{-}(\mathbf{4}) \quad (2)$$

Dilution is a driving force for reaction 2. Species **4** as shown is analogous to the postulated compound II of haloperoxidases [22, 23], although the recently suggested actual speciation of iron(IV) TAMLs in aqueous solution is significantly more complex [16].

Control experiments with **2** generated from a sodium salt of **1** in the presence of 0.5 equivalents of H_2O_2 or ^{t}BuOOH have shown that **2** is rapidly reduced by electron donors to afford **1**. When an orange solution of **1** (1×10^{-4} M) at pH 8 (0.01 M phosphate buffer) is treated with ^{t}BuOOH, the solution turns dark and new bands appear at 800 and 1100 nm with a shoulder at 540 nm [figure 1(a)]. It takes ca. 10 min to achieve this conversion at 25 °C. TAML-catalyzed degradation of Orange II by peroxides was studied in detail previously [24] and therefore it was used in this work. Orange II has a strong band around 480 nm and does not absorb light at 800 nm. Therefore, both the dye degradation and the

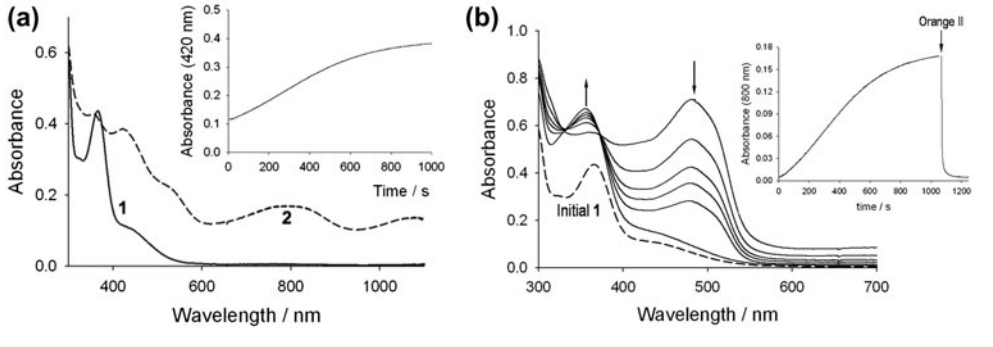

Figure 1. (a) Formation of **2** from **1** and 0.5 equiv ^{t}BuOOH. Inset to (a) shows kinetics of the formation of **2**. (b) Dashed line is the spectrum of **1** before adding ^{t}BuOOH. The solution of Orange II (5×10^{-5} M) was added after the formation of **2** was complete and the solid spectra visualize the dye bleaching. Inset to (b) shows a rapid decrease in absorbance at 800 nm due to reduction of **2** restoring the spectrum of **1** which is affected by the products of degradation of Orange II. Conditions: [**1**] 1×10^{-4} M, [^{t}BuOOH] 5×10^{-5} M, pH 8 (0.01 M phosphate), and 25 °C.

reduction of **2** into **1** could be confirmed in one experiment [figure 1(b)]. Both processes occur at similar rates. Similar bleaching of Orange II by **2** was observed when H_2O_2 (0.5 eq) was used instead of ^{t}BuOOH.

3.2. *Stopped-flow kinetic studies of reactions of 2 with p-XC$_6$H$_4$SMe*

Thianisole reacts with **2** instantaneously at room temperature. Dimer **2** is reduced back into **1** producing methyl phenyl sulfoxide as confirmed by HPLC. Kinetics of the reduction of **2** into **1** by *p*-XC_6H_4SMe was studied using stopped-flow spectroscopy in excess of sulfides to ensure pseudo-first-order conditions. A decrease in the absorbance of **2** (ca. 10^{-5} M) at 420 nm was registered. Exponential kinetic traces as shown in figure 2 were generated in all cases studied. Satisfactory first-order kinetics was observed in a matter of 3–4 half-lives. The pseudo-first-order rate constants k_{obs} were measured at different concentrations of thioanisoles and revealed hyperbolic dependencies such as in figure 3 for all *p*-XC_6H_4SMe studied. Plots k_{obs}^{-1} *versus* $[XC_6H_4SMe]^{-1}$ were straight lines with nonzero intercepts consistent with rate law 3, which agrees with a mechanism involving the formation of an intermediate produced from **2** and thioanisole followed by the rate-limiting step. Interestingly, the same rate law was established for the reaction between the same partners in acetonitrile at −40 °C [15].

$$k_{obs} = \frac{ab[\text{ArSMe}]}{1 + b[\text{ArSMe}]} \tag{3}$$

The *a* and *b* parameters of equation (3) were calculated for all thioanisoles used in this study by fitting the data such as in figure 3 to equation (3) and the corresponding values are summarized in table 1. The rate law 3 and the dimeric structure of **2** combined suggest several mechanistic possibilities, some of which are included in table 2. Mechanism M1 assumes that the intact dimer **2** coordinates reversibly an organic sulfide followed by rate-limiting electron transfer to afford a radical cation $MeArS^{+\cdot}$ which is then rapidly transformed into a sulfoxide through a sequence of events proposed elsewhere [25].

Mechanism M2 (table 2) involves a reversible conversion of dimer **2** into a monomeric reactive Fe^{IV}-sulfide adduct as a result of a bridge cleavage by the nucleophilic organic sulfide followed by the electron transfer step. Mechanism M3 assumes that sulfide attack at dimer **2** causes its disproportionation that leads to the iron(V)oxo species coordinated by sulfide and an iron(III) derivative. The iron(V)oxo species may be involved in a concerted oxygen atom transfer affording sulfoxide and iron(III). Mechanism M4 is based on the assumption that dimer **2** is noticeably less reactive than a monomeric form such as **4** in equation (2). The **4** monomer forms a reactive intermediate with sulfide followed by an electron transfer step. There is one essential feature that distinguishes M4 from mechanisms M1–M3. If the equilibrium driven by K_4 is shifted strongly to the left (dimer **2** is a dominating species in solution), the reaction should have a kinetic order of one-half in the oxidant. Kinetic results obtained under the steady-state conditions, which are described below, will highlight the importance of additional mechanism M5, which is actually a combination of M1 and M4.

The corresponding kinetic equations for all mechanisms in table 2 shows that the kinetic parameter *a* is equal or proportional to the rate constant k_2, which corresponds to the electron (or atom in M3) transfer from sulfide at Fe^{IV} (or Fe^{V} in M3). The parameter *b*,

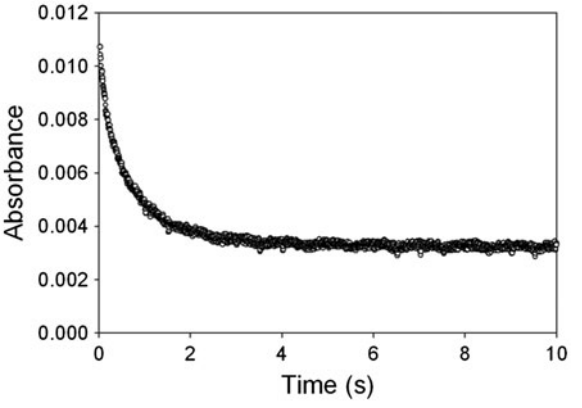

Figure 2. Kinetic trace corresponding to reduction of **2** (1×10^{-5} M) by thioanisole (5×10^{-5} M) as monitored at 420 nm by stopped-flow spectroscopy. **2** was made from **1** and H_2O_2 prior to the addition of sulfide. Conditions: pH 8 (0.01 M phosphate) and 25 °C.

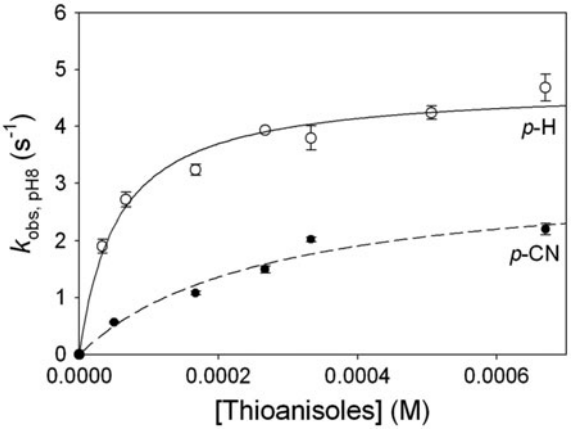

Figure 3. Pseudo-first-order rate constants k_{obs} for the reduction of **2** into **1** against different concentrations of *p*-XC_6H_4SMe (○, X=H; ●, X=CN). Solid and dashed lines are calculated curves using the best-fit parameters of equation (3) summarized in table 1. Conditions: pH 8 (0.01 M phosphate) and 25 °C.

Table 1. Parameters *a*, *b*, and *ab* of equation (3) experimentally obtained for TAML compound **2** at 25 °C, pH 8 in 0.01-M phosphate. Compound **2** (~1 (10^{-5} M) was obtained from **1** and H_2O_2 prior to addition of methyl aryl sulfides.

X in *p*-XC_6H_4SMe	$10^{-3} \times b/M^{-1}$	a/s^{-1}	$10^{-4} \times ab/M^{-1}\ s^{-1}$
OCH_3	25 ± 7	4.8 ± 0.3	12
CH_3	16 ± 3	4.6 ± 0.2	7.4
H	24 ± 4	4.3 ± 0.2	10.3
Cl	14 ± 6	4.1 ± 0.5	5.7
CN	4 ± 1	3.2 ± 0.5	1.3
NO_2			1.2[a]

[a]Value extrapolated from the Hammett plot in figure 4.

Table 2. Mechanistic options for oxidation of methyl aryl sulfides by **2**; all but M4 are consistent with the rate law 3.

M1	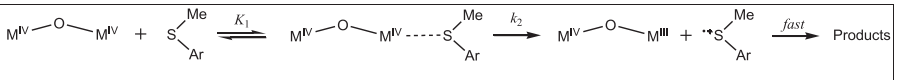
	$k_{obs} = \frac{k_2 K_1[S]}{1 + K_1[S]}$; $a = k_2$, $b = K_1$
M2	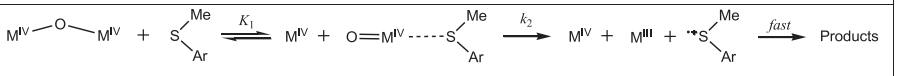
	$k_{obs} = \frac{0.5 k_2 K_1 [M^{IV}]^{-1}[S]}{1 + K_1[M^{IV}]^{-1}[S]}$; $a = 0.5k_2$, $b = K_1[M^{IV}]^{-1}$
M3	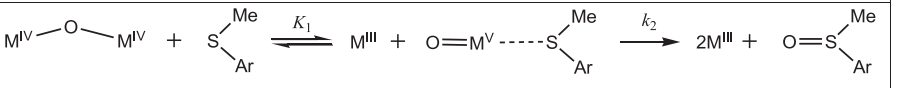
	$k_{obs} = \frac{0.5 k_2 K_1 [M^{III}]^{-1}[S]}{1 + K_1[M^{III}]^{-1}[S]}$; $a = 0.5k_2$, $b = K_1[M^{III}]^{-1}$
M4	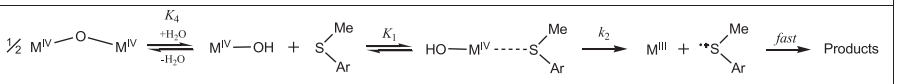
	$-\frac{d[2]}{dt} = \frac{k_2[S]\sqrt{K_4 M_t}}{\frac{k_{-1}+k_2}{k_1}+[S]}$; $-\frac{d[2]}{dt} = \frac{k_2 K_1[S]\sqrt{K_4 M_t}}{1+K_1[S]}$
M5	M1 + M4
M6	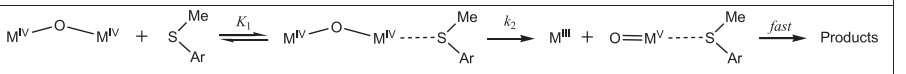

which is equal or proportional to K_1, characterizes an ability of sulfides to coordinate iron. The product ab, which is proportional to k_2K_1, links the reaction conditions at low concentrations of p-XC_6H_4SMe and therefore corresponds to effective second-order rate constants for the interaction between iron(IV) species and thioanisoles. Accordingly, figure 4 compares the substituent effects of X in p-XC_6H_4SMe on a, b, and ab in terms of the Hammett formalism. As shown, all kinetic parameters decrease from electron-rich to electron-poorer sulfides, i.e. electron-withdrawing substitutions disfavor the reaction via all possible channels. Both electron transfer rates and binding of sulfides to iron(IV) decrease as the basicity of sulfides drops. The best Hammett correlation is observed for log (a/a_H), which is in fact ~log (k_2/k_{2H}). The ρ slope of −0.18 is however very low pointing to an insignificant sensitivity of the intramolecular electron transfer step to electronic effects in sulfides when the reaction is run in water. The ρ of −0.18 suggests an additional mechanistic option (M6) similar to M3. The rate-limiting step of M6 is the disproportion during the oxo bridge cleavage of **2** to afford iron(III) and iron(V) species, the latter rapidly oxidizing sulfide (table 2).

Parameter *b*, which is associated with binding of sulfides to iron(IV) in multiple ways, is noticeably more sensitive to the electronic effects ($\rho = -0.79$). As anticipated, the binding weakens for electron-poor sulfides. The *ab* product, which reflects contributions from both the binding and the rate-limiting electron transfer step, has the most negative ρ of ca. −1. Its absolute value is however still appreciably lower than that of −2.1 observed for the oxidation of the same sulfides to sulfoxides by the TAML iron(V)oxo species in wet MeCN as solvent [15]. The analytical expression 4 for the line was used to estimate the *ab* value of $(1.2 \pm 0.8) \times 10^4$ M^{-1} s^{-1} for *p*-$NO_2C_6H_4SMe$ using the Hammett σ constant for NO_2 of 0.78 [26].

$$\log(ab/ab_H) = -(0.16 \pm 0.07) - (0.98 \pm 0.21) \times \sigma \quad (4)$$

3.3. *Kinetics of 1-catalyzed oxidation of 4-nitrothioanisole by hydrogen peroxide under the steady-state conditions*

The previous section summarizes the results of single-turnover kinetic studies of oxidation of organic sulfides by iron(IV) species **2** in aqueous solution. Complex **2** does not absorb visible light strongly and therefore such studies in excess of electron donors were possible for colorless thioanisoles *p*-XC_6H_4SMe with X=MeO, Me, H, Cl, and CN. The nitro derivative *p*-$NO_2C_6H_4SMe$ could not be investigated similarly because it has a band at 350 nm. In contrast, kinetic studies of **1**-*catalyzed* oxidation of *p*-$NO_2C_6H_4SMe$ by H_2O_2 are feasible as opposed to the other colorless thioanisoles. The reaction between **1** and H_2O_2 affords **2** in a more than 80% yield at pH below 10 [12] and therefore we decided to compare the rate constants obtained under the steady-state and single-turnover conditions, the latter being available for *p*-$NO_2C_6H_4SMe$ from extrapolation using equation (4). Under the catalytic conditions, *p*-$NO_2C_6H_4SMe$ is oxidized by H_2O_2 into the corresponding sulfoxide confirmed by HPLC and GC–MS after the reaction was completed. The oxidation of *p*-$NO_2C_6H_4SMe$ into *p*-$NO_2C_6H_4SOMe$ is a very clean process. As seen in figure 5, the sulfide is gradually converted into the sulfoxide, which has a maximal absorbance at 280 nm. Two isosbestic points hold at 239 and 305 nm suggesting no accumulation of other absorbing intermediates. The kinetic data collected at 350 and 280 nm match perfectly. No further oxidation of the sulfoxide into sulfone was observed under the reaction conditions used (pH 8, 25 °C).

We have performed several kinetic studies of TAML-catalyzed oxidations of different targets (D) by peroxides [16, 24, 27–31]. The oxidations were first order in the catalyst at concentrations below 10^{-6} M. Mixed orders in H_2O_2 and D were established as in equation (5).

$$-\frac{d[D]}{dt} = \frac{k_I k_{II}[H_2O_2][D]}{k_{-I} + k_I[H_2O_2] + k_{II}[D]}\left[Fe^{III}\right] \quad (5)$$

Equation (5) is consistent with a minimalistic reaction mechanism presented in scheme 1. If the oxidation of D occurs "in the k_{II} kinetic regime" when $k_I[H_2O_2] >> k_{-I} + k_{II}[D]$ at high concentrations of H_2O_2, equation (4) simplifies to $-d[D]/dt = k_{II}[D][Fe^{III}]$ and the second-order rate constant k_{II} should be similar to the product *ab* (table 1). The fact that the oxidation of iron(III) TAML by H_2O_2 may afford an iron(V) intermediate [14, 27] is kinetically unimportant because the reactivity of Fe^V to sulfides is by four orders of magnitude higher

than that of Fe^{IV} [15] and under the steady-state conditions, the rate-limiting step should be the oxidation by Fe^{IV}. The reader may find more detailed justification elsewhere [16].

However, the rate of oxidation deviated from linearity at higher concentrations of TAML catalysts in certain cases and this issue is addressed here because the iron(IV) dimeric

$$Fe^{III}\text{-TAML} + ROOH \underset{k_{-1}}{\overset{k_1}{\rightleftharpoons}} \text{(Oxidized TAML)}$$

$$\text{(Oxidized TAML)} + \text{Substrate} \xrightarrow{k_{II}} Fe^{III}\text{-TAML} + \text{Product}$$

$$\text{Primary Product} \xrightarrow{fast} \rightarrow \rightarrow \text{Final Product(s)}$$

Scheme 1. General mechanism of catalysis by TAML activators in aqueous media.

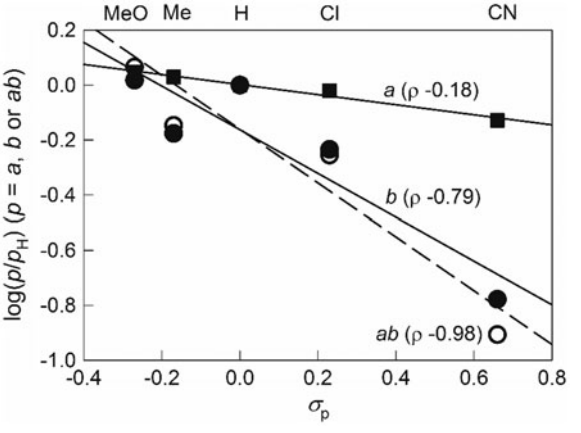

Figure 4. Hammet plots of parameters of equation (3) in a log (p/p_H) form (p = a, b, or ab) against σ_p of p-substituted thianisoles for their oxidation by **2** at pH 8 and 25 °C. Data are from table 1.

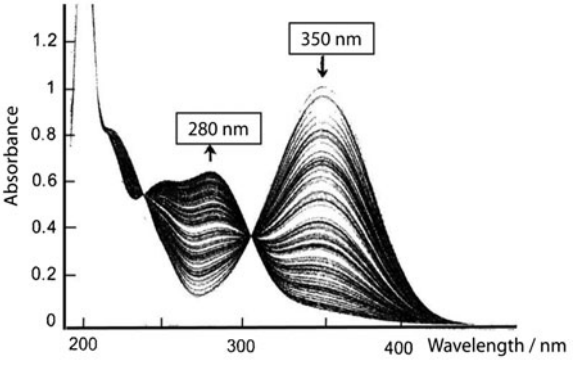

Figure 5. Spectral changes during **1**-catalyzed oxidation of p-$NO_2C_6H_4SMe$ (7.1×10^{-5} M) by H_2O_2 (0.04 M). Other conditions: [**1**] = 2.3×10^{-7}, pH 8, and 25 °C.

species dominate at *milli*molar concentrations in aqueous solution at pH below 10. The catalysis is however performed using *micro*molar and lower concentrations of TAMLs and therefore dimer **2** could undergo monomerization to form **4** as in equation (2).

It has been confirmed that the oxidation of *p*-$NO_2C_6H_4SMe$ follows "normal" kinetics under the conditions typically used for catalysis by TAMLs. Figure 6 shows that the reaction rate is directly proportional to the concentration of **1** below 10^{-6} M. Figure 7 illustrates a hyperbolic dependence of the rate on $[H_2O_2]$. The inset to figure 7 shows that the inverse rate is proportional to $[H_2O_2]^{-1}$ with a positive intercept as predicted by equation (4). Assuming that k_{-I} is negligible [11], the rate constants k_I and k_{II} of 167 ± 20 and $(1.6 \pm 0.2) \times 10^5$ M^{-1} s^{-1}, respectively, have been calculated. The k_I value agrees with that of 260 M^{-1} s^{-1} obtained previously using a cyclometalated ruthenium(II) dye as an electron

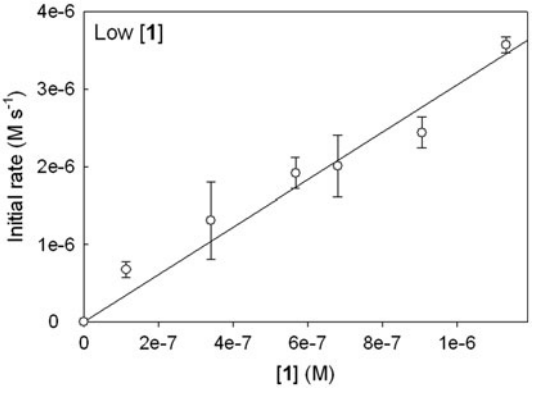

Figure 6. Linear dependence of initial rates of oxidation of *p*-$NO_2C_6H_4SMe$ on concentration of **1** below 10^{-6} M at [sulfide] 2.4×10^{-5} M, $[H_2O_2]$ 0.4 M, pH 8 (0.01 M phosphate), and 25 °C.

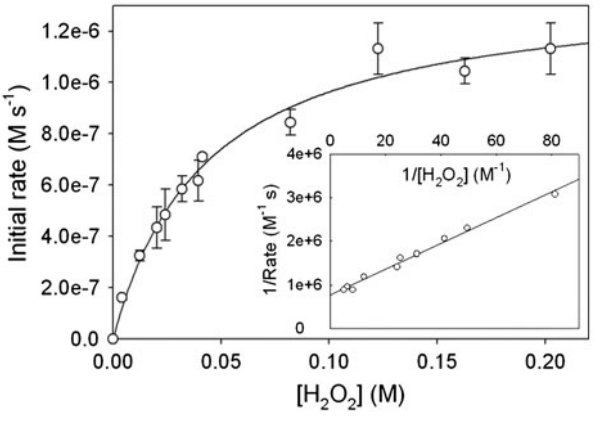

Figure 7. Initial rate of oxidation of 4-nitrothioanisole by H_2O_2 catalyzed by **1** as a function of peroxide concentrations. Inset is the corresponding double reciprocal plot. Conditions: [**1**] 2.3×10^{-7} M, [4-nitrothioanisole] 7.1×10^{-5} M, pH 8 (0.01 M phosphate), and 25 °C.

donor under the same conditions [27]. The k_{II} value appeared by one order of magnitude higher than *ab* estimated from the Hammett plot.

To resolve the rate controversy, we have measured initial rates of oxidation of *p*-$NO_2C_6H_4SMe$ by H_2O_2 in the broadest range of concentrations of **1** at a high concentration of H_2O_2 to ensure that the limiting rate expression $-d[D]/dt = k_{II}[D][Fe^{III}]$ holds. The data presented in figure 8, which covers a 100-fold concentration range, indicate that a nonlinear dependence is observed. The reaction order in **1** changes from one (figure 6) to one-half [figure 8(b)] at lower and higher concentrations of the catalyst, respectively. This observation is consistent with the occurrence of the postulated equation (2). The fraction of monomeric species such as **4** increases on dilution and, if the reactivity of the monomeric species is appreciably higher than that of the dimeric counterparts, the dependence shown in [figure 8(a)] can be rationalized quantitatively. The corresponding mechanism assumes the coexistence of both active monomeric and dimeric species (scheme 2) and results in equation (6) for the dependence of the reaction rate on the total catalyst concentration $M_t = [M] + 2[M_2]$.

$$-\frac{d[D]}{dt} = \frac{[D]}{8K_d}\left\{(2k_m - k_d) \times \left(\sqrt{8K_dM_t + 1} - 1\right) + 4k_dK_dM_t\right\} \quad (6)$$

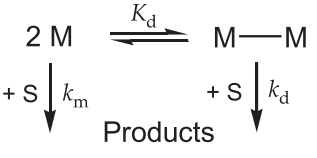

Scheme 2. A reaction scheme involving monomeric M and dimeric M–M oxidized intermediates in catalysis by TAMLs (see text for details).

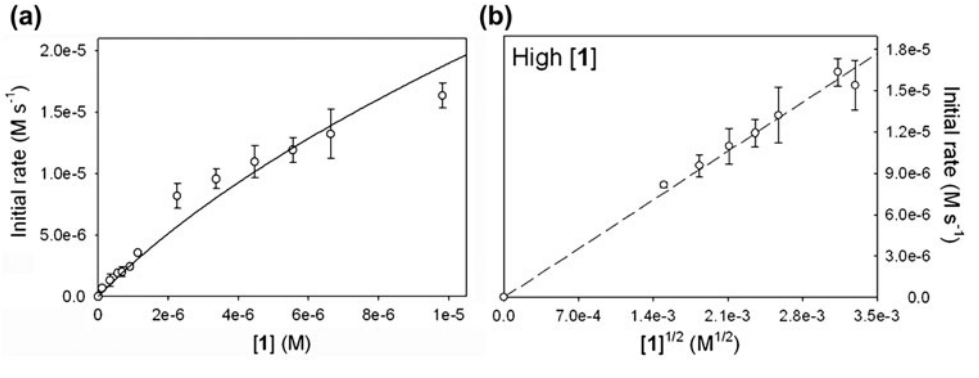

Figure 8. (a) Deviation from linearity of the initial rate for oxidation of *p*-$NO_2C_6H_4SMe$ (2.4×10^{-5} M) by H_2O_2 (0.4 M) as a function of concentrations of **1** covering a 100-fold range. The solid line was calculated using the best-fit values of k_d and K_d (see text for details). (b) The rate as a linear function of a square root of [**1**] at [**1**] > 1×10^{-6} M. Conditions: pH 8 (0.01 M phosphate) and 25 °C.

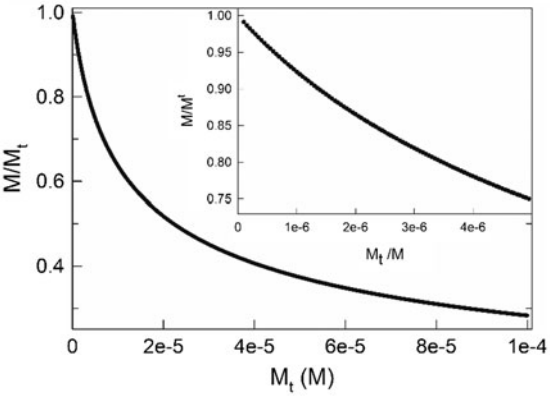

Figure 9. Fraction of the monomeric form M of iron(IV) as a function of total iron concentration calculated using $K_d = 4.5 \times 10^5$ M^{-1}. Inset is the same dependence at low M_t.

Equation (6) includes terms proportional both to M_t and $\sqrt{M_t}$, the latter being negligible at lower catalyst concentrations. Equation 6 is in qualitative agreement with the data presented in figure 8 and therefore it was used for fitting the data. The value of k_m ($(13 \pm 1) \times 10^4$ M^{-1} s^{-1}) was determined directly from the data collected at the lowest concentrations of the catalyst (figure 6) and therefore k_d and K_d, i.e. the rate constant for the dimer and the dimerization constant, respectively, were found in the fitting routine. The values of k_d and K_d equal $(0.32 \pm 0.01) \times 10^4$ M^{-1} s^{-1} and $(4.5 \pm 0.5) \times 10^4$ M^{-1}, respectively. The value of k_d for *p*-$NO_2C_6H_4SMe$ obtained in the fit should be compared to that of $(1.2 \pm 0.8) \times 10^4$ M^{-1} s^{-1} estimated from the Hammett plot in figure 4. Though the latter is slightly higher than k_d obtained from the data in figure 8, they are rather close taking into account experimental uncertainties. The observed difference may be due to the fact that k_m and k_d differ by almost two orders of magnitude and the monomerization via equation (2) could not be taken into consideration in the single-turnover experiments.

The value of equilibrium constant K_d has been used to calculate the concentration profile for a relative amount of the monomeric form in solution at pH 8 (figure 9). The relative amount of the monomeric form is higher than 90% at concentrations below 1.4×10^{-6} M and is 50% at 2.2×10^{-5} M. Thus, dilute solutions of TAMLs should preferably be used in kinetic studies to avoid complicating kinetic analysis association phenomena.

4. Conclusion

Reactive iron(IV) species produced from TAML activators in the presence of peroxides may undergo spontaneous dimerization when the catalyst concentration exceeds 10^{-6} M in aqueous solution at pH 8. The dimerization is negligible in water when more dilute solutions of TAML activators are used. The dimerization may cause a switch of the reaction order in the catalysts from 1 to ½, though mixed reaction order may also be observed. The results presented here support our previous assumption that reactive monomeric iron(IV) TAMLs are not affected by aggregation to any significant extent when used at

concentrations below 10^{-6} M in water [16]. This study would not be possible without using the stopped-flow spectroscopy, the technique which one of us (ADR) learned from Rudi (van Eldik) when we all were much younger [32].

Acknowledgement

ADR thanks Genoa R. Warner for critical reading of the manuscript and helpful comments.

Disclosure statement

No potential conflict of interest was reported by the authors.

Funding

Operating support is acknowledged from the Heinz Endowments (T.J.C.); the Institute for Green Science (T.J.C.); the Environmental Protection Agency [grant number RD 83 to T.J.C.].

References

[1] M. Costas, M.P. Mehn, M.P. Jensen, L. Que Jr. *Chem. Rev.*, **104**, 939 (2004).
[2] S.V. Kryatov, E.V. Rybak-Akimova, S. Schindler. *Chem. Rev.*, **105**, 2175 (2005).
[3] I.V. Korendovych, S.V. Kryatov, E.V. Rybak-Akimova. *Acc. Chem. Res.*, **40**, 510 (2007).
[4] L. Que. *Acc. Chem. Res.*, **40**, 493 (2007).
[5] A.D. Ryabov. *Adv. Inorg. Chem.*, **65**, 118 (2013).
[6] A.R. McDonald, L. Que. *Coord. Chem. Rev.*, **257**, 414 (2014).
[7] W. Nam, Y.-M. Lee, S. Fukuzumi. *Acc. Chem. Res.*, **47**, 1146 (2014).
[8] T.J. Collins. *Acc. Chem. Res.*, **27**, 279 (1994).
[9] T.J. Collins. *Acc. Chem. Res.*, **35**, 782 (2002).
[10] T.J. Collins, S.K. Khetan, A.D. Ryabov, In *Handbook of Green Chemistry*, P.T. Anastas, R.H. Crabtree (Eds), pp. 39–77. Wiley-VCH Verlag GmbH & KgaA, Weinheim (2009).
[11] A.D. Ryabov, T.J. Collins. *Adv. Inorg. Chem.*, **61**, 471 (2009).
[12] A. Chanda, X. Shan, M. Chakrabarti, W. Ellis, D. Popescu, F. Tiago de Oliveira, D. Wang, L. Que Jr., T.J. Collins, E. Münck, E.L. Bominaar. *Inorg. Chem.*, **47**, 3669 (2008).
[13] A. Chanda, F. Tiago de Oliveira, T.J. Collins, E. Munck, E.L. Bominaar. *Inorg. Chem.*, **47**, 9372 (2008).
[14] D.-L. Popescu, M. Vrabel, A. Brausam, P. Madsen, G. Lente, I. Fabian, A.D. Ryabov, R. van Eldik, T.J. Collins. *Inorg. Chem.*, **49**, 11439 (2010).
[15] S. Kundu, J. Van Kirk Thompson, A.D. Ryabov, T.J. Collins. *J. Am. Chem. Soc.*, **133**, 18546 (2011).
[16] S. Kundu, M. Annavajhala, I.V. Kurnikov, A.D. Ryabov, T.J. Collins. *Chem. Eur. J.*, **18**, 10244 (2012).
[17] D.D. Perrin, W.L.F. Armarego. *Purification of Laboratory Chemicals*, 3rd Edn, Pergamon Press, Oxford, New York (1988).
[18] A. Ghosh. Design, synthesis and mechanistic studies of Iron-TAML catalytic activators of hydrogen peroxide and a new activation chemistry of dioxygen by iron. PhD thesis, Department of Chemistry, Carnegie Mellon University, Pittsburgh, PA (2004).
[19] P. George. *Biochem. J.*, **54**, 267 (1953).
[20] A. Ghosh, A.D. Ryabov, S.M. Mayer, D.C. Horner, D.E. Prasuhn Jr., S. Sen Gupta, L. Vuocolo, C. Culver, M.P. Hendrich, C.E.F. Rickard, R.E. Norman, C.P. Horwitz, T.J. Collins. *J. Am. Chem. Soc.*, **125**, 12378 (2003).
[21] A. Ghosh, F. Tiago de Oliveria, T. Toshihiro Yano, T. Nishioka, E.S. Beach, I. Kinoshita, E. Münck, A.D. Ryabov, C.P. Horwits, T.J. Collins. *J. Am. Chem. Soc.*, **127**, 2505 (2005).
[22] K.L. Stone, L.M. Hoffart, R.K. Behan, C. Krebs, M.T. Green. *J. Am. Chem. Soc.*, **128**, 6147 (2006).
[23] J. Terner, V. Palaniappan, A. Gold, R. Weiss, M.M. Fitzgerald, A.M. Sullivan, C.M. Hosten. *J. Inorg. Biochem.*, **100**, 480 (2006).
[24] N. Chahbane, D.-L. Popescu, D.A. Mitchell, A. Chanda, D. Lenoir, A.D. Ryabov, K.-W. Schramm, T.J. Collins. *Green Chem.*, **9**, 49 (2007).
[25] S. Kobayashi, M. Nakano, T. Kimura, A.P. Schaap. *Biochemistry*, **26**, 5019 (1987).

[26] C. Hansch, A. Leo, R.W. Taft. *Chem. Rev.*, **91**, 165 (1991).
[27] A. Ghosh, D.A. Mitchell, A. Chanda, A.D. Ryabov, D.L. Popescu, E. Upham, G.J. Collins, T.J. Collins. *J. Am. Chem. Soc.*, **130**, 15116 (2008).
[28] D. Banerjee, F.M. Apollo, A.D. Ryabov, T.J. Collins. *Chem. Eur. J.*, **15**, 10199 (2009).
[29] W.C. Ellis, C.T. Tran, R. Roy, M. Rusten, A. Fischer, A.D. Ryabov, B. Blumberg, T.J. Collins. *J. Am. Chem. Soc.*, **132**, 9774 (2010).
[30] D.A. Mitchell, A.D. Ryabov, S. Kundu, A. Chanda, T.J. Collins. *J. Coord. Chem.*, **63**, 2605 (2010).
[31] G. Warner, M. Mills, C. Enslin, S. Pattanayak, C. Panda, S. Sen Gupta, A.D. Ryabov, T.J. Collins. *Chem. Eur. J.* **21**, 6226 (2015).
[32] A.D. Ryabov, L.G. Kuz'mina, V.A. Polyakov, G.M. Kazankov, E.S. Ryabova, M. Pfeffer, R. van Eldik. *J. Chem. Soc., Dalton Trans.*, 999 (1995).